Received: 31 May 2024 | Revised: 14 August 2024 | Accepted: 16 August 2024

DOI: 10.1002/pamm.202400203

RESEARCH ARTICLE

Thermomechanical analysis of strain recovery in shape memory alloys under variable non-isothermal conditions

Stefan Descher[1] | **Philipp Krooß**[2] | **Felix Ewald**[2] | **Detlef Kuhl**[1]

[1]Institute of Structural Mechanics, University of Kassel, Kassel, Germany

[2]Institute of Materials Engineering, Metallic Materials, University of Kassel, Kassel, Germany

Correspondence
Stefan Descher, Institute of Structural Mechanics, University of Kassel, 34125, Kassel, Germany.
Email: descher@uni-kassel.de

Abstract

The present work focuses on size dependencies in thermo-mechanical testing of shape memory alloys and a phenomenon occurring for direction-dependent activation. Emphasis is on strain recovery which is enabled by a martensite-to-austenite transformation, modeled using a phenomenological evolution equation. In transient numerical studies performed with the finite element method for a non-isothermal tension testing case, the influence of the FOURIER and STEFAN number is investigated. The results indicate that, in experiments, the FOURIER number should ideally be much greater than ten to prevent falsification by the current STEFAN number. An additional study is carried out for the activation of a beam in its thickness direction. It shows that the gradient in transformation causes bending, which can only be considered in simulations by adequate spatial resolution.

1 | INTRODUCTION

A major reason for the application of shape memory alloys (SMAs) is to utilize the one-way effect. It allows the recovery of plastic strains that are mechanically introduced into the material, by thermal activation due to heating. The underlying process is a phase transformation from a martensitic phase to an austenitic phase that occurs in a specific temperature range. A popular application of SMAs are actuators, often found in aviation [1] and automotive industry, or as smart reinforcements in novel materials of civil engineering, see refs. [2, 3]. As found out in the preceding thermodynamic studies of the present work in ref. [4], latent heat effects play a key role in this activation process. The heat sink caused by the martensite-austenite phase transformation during activation causes a transformation interface to move through the material. This highly depends on the local heating rate, that is reached during activation. To further study this behavior, in the present work, mechanical coupling is realized. Studies are carried out for a characteristic non-isothermal tension test, which allows to give advice for experimental testing. Since dimensionless numbers are used, results can be transferred to any type of sample. This might be the standard dog bone type of sample [5], single wires [6], or even cables [7].

Performing experiments for recording typical stress-strain-temperature curves requires a special setup. This is, for example, a tension testing machine equipped with a furnace surrounding the specimen and the mounts, as can be seen in Figure 1 left. In improved systems, the furnace is designed in a way to ensure a temperature distribution that is as homogeneous as possible. One method to reach this goal is to design the heating cell axisymmetric and use a spiral heating, as shown in Figure 1 right. Particularly in experiments that investigate temperature dependencies and therefore rely on

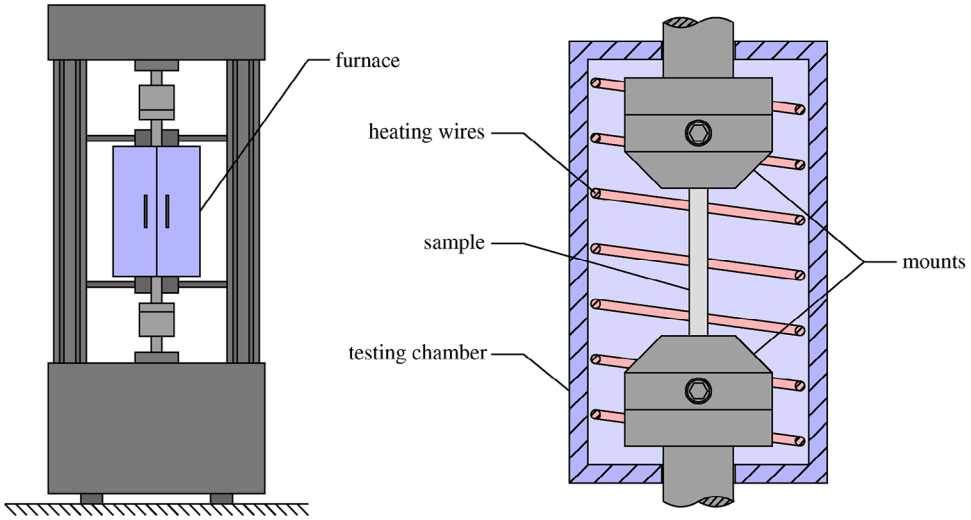

FIGURE 1 Standard non-isothermal tension testing configuration. Left: tensile testing machine with furnace. Right: interior of the furnace with spiral heating for uniform heat distribution.

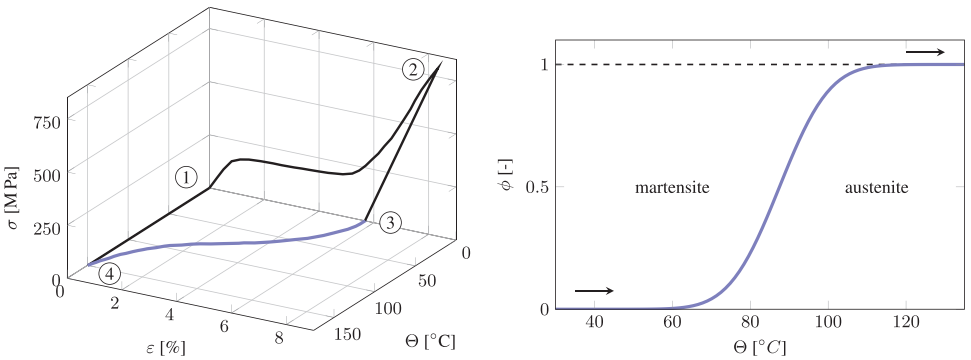

FIGURE 2 Left: example of a stress-strain-temperature curve for NiTi, as given in ref. [1]. Right: solution of the phase indicator function generated by solving Equation (1), further described in ref. [4].

a change of temperature, this ensures small temperature gradients in the cell. That this is not the case for the sample is well known since there is a heat conduction process from its surface to the core causing thermal lag. For minimization of this effect, the sample size should generally be chosen to be as small as possible, or the rate of temperature change should be small. The purpose of the present work is giving guidance in the process of choosing sample sizes and heating rates for non-isothermal testing of SMAs. Novelty is that latent heat is considered, which is a key phenomenon for SMAs and therefore distinguishes them from standard steels.

2 | MODELING AND SIMULATION APPROACH

The model applied in the present work is formulated to exclusively describe the process of strain recovery. In a typical stress-strain-temperature curve, as shown in Figure 2 left, it is following the isothermal prestreching section, which is the process between points 1, 2, and 3. Thereafter, the temperature is increased which causes the strains to reduce, as can be observed between points 3 and 4. The effect enabling strain recovery is a phase transformation from martensite to austenite.

In the present work, it is modeled using a phase indicator ϕ, which for $\phi = 0$ represents martensite and for $\phi = 1$ represents austenite. It is derived directly from data determined with differential scanning calorimetry (DSC). A detailed

description is given in the preceding work [4]. Core is the evolution equation

$$\dot{\phi}(\Theta,\dot{\Theta}) = \max\left(0, \frac{\mathrm{d}\phi}{\mathrm{d}\Theta}\frac{\partial\Theta}{\partial t}\right), \tag{1}$$

which only allows an increase of ϕ, meaning that the phase transformation is irreversible. Next to the temperature rate $\dot{\Theta}$, which is determined in the time integration scheme, it also contains the analytical derivative

$$\frac{\mathrm{d}\phi}{\mathrm{d}\Theta} = \sqrt{\frac{4\ln 2}{\pi\Delta\Theta_{tr}}}\exp\left(-4\ln 2\frac{(\Theta_{tr}-\Theta)^2}{\Delta\Theta_{tr}^2}\right). \tag{2}$$

It is based on two model parameters, the transformation temperature range $\Delta\Theta_{tr}$ and transformation temperature Θ_{tr}. The underlying phase indicator function used for the current work is plotted in Figure 2 right. Considering a standard enthalpy method [8], for example, known from phase-field methods [9], the rate of change of ϕ is connected to the magnitude of heat sink $\dot{Q}_{tr}$, caused by the endothermic phase transformation. The resulting energy equation is

$$\rho c\,\dot{\Theta} = \nabla\cdot(\lambda\nabla\Theta) \underbrace{-\rho\Delta h_{tr}\frac{\partial\phi}{\partial t}}_{\dot{Q}_{tr}}, \tag{3}$$

based on density ρ, thermal conductivity λ and the phase transformation enthalpy Δh_{tr}. Coupling the phase transformation mechanically is achieved by strain decomposition in the constitutive law for the CAUCHY stress tensor $\boldsymbol{\sigma}$, therefore, the balance of momentum is given by

$$\rho\ddot{\boldsymbol{u}} = \mathrm{div}\underbrace{\left[\mathbb{C} : (\boldsymbol{\varepsilon}_u - \boldsymbol{\varepsilon}_{th}(\Theta) - \boldsymbol{\varepsilon}_{tr}(\phi))\right]}_{\boldsymbol{\sigma}}. \tag{4}$$

In this equation, the constitutive tensor $\mathbb{C}$, displacement-related strains $\boldsymbol{\varepsilon}^u = \nabla^{sym}\mathbf{u}$ and thermal strains $\boldsymbol{\varepsilon}_{th} = \alpha_{th}(\theta - \theta_{ref})$ as well as the linear connection between the state of transformation and the corresponding strains

$$\boldsymbol{\varepsilon}_{tr}(\phi) = -\boldsymbol{\varepsilon}_0\phi \tag{5}$$

are used. It is based on the prestrain tensor $\boldsymbol{\varepsilon}_0$, which represents the strains that were brought into the material by prestretching. Its magnitude is controlled by the scalar quantity ε_0, as shown by the following equation:

$$\boldsymbol{\varepsilon}_0 = \varepsilon_0\begin{bmatrix}1 & 0 & 0\\ 0 & 1 & 0\\ 0 & 0 & 1\end{bmatrix}. \tag{6}$$

It means transformation strains are released volumetrically, other options are possible as well, further discussed in ref. [3]. The resulting thermo-mechanical field problem is solved using the Finite-Element-Method. A self-developed, geometrically linear solver based on p-FEM using LAGRANGE polynomials and GAUSS integration is used. In the simulations performed for the present work, the polynomial degree is set to two, four GAUSS-points are used per element. For time integration, the NEWMARK-α scheme is applied.

3 | INITIAL-BOUNDARY VALUE PROBLEMS

Subject of study is a tensile testing case in which during strain recovery, longitudinal deformation of the sample is prevented. This causes stresses to build up, which cause a retention force that can be related to strain release. It is an axisymmetric setup, as shown in Figure 3 left. Further investigations are performed for a plane stress beam case, that is depicted in Figure 3 on the top right. It allows highlighting a directional-dependent phenomenon relevant to certain

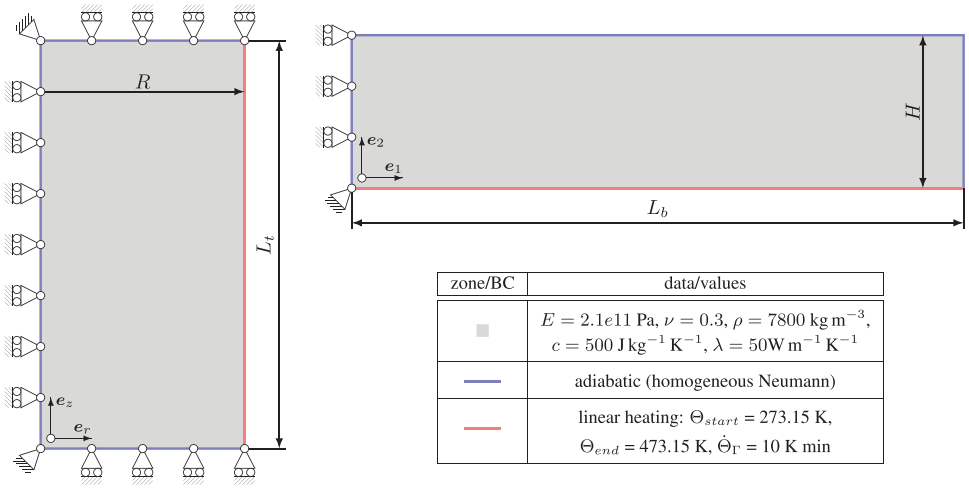

zone/BC	data/values
	$E = 2.1e11$ Pa, $\nu = 0.3$, $\rho = 7800\,\mathrm{kg\,m^{-3}}$, $c = 500\,\mathrm{J\,kg^{-1}\,K^{-1}}$, $\lambda = 50\mathrm{W\,m^{-1}\,K^{-1}}$
	adiabatic (homogeneous Neumann)
	linear heating: Θ_{start} = 273.15 K, Θ_{end} = 473.15 K, $\dot{\Theta}_\Gamma$ = 10 K min

FIGURE 3 Definition of the tensile testing case (left) and the beam case (top right) as well as material data used in the simulations.

parameter settings. Since the material that was investigated in the DSC scans is a newly composed, processed by Laser Power Bed Fusion, Nickel-Titanium-Hafnium (NiTiHf, see ref. [4]) alloy, no other material data is known. For this reason, as can be seen in the table of Figure 3, the thermomechanical parameters for steel had to be chosen, since they reflect the correct magnitude. However, numerical studies are performed using dimensionless numbers, which allows transferring results to the exact parameter relations.

Both cases start from the static state at $\Theta = \Theta_{start}$, one boundary performs a linear heating ramp to pass the temperature range $\Delta\Theta = \theta_{end} - \theta_{start}$ in the characteristic time $\tau = \frac{\Delta\Theta}{\dot{\Theta}_\Gamma}$, therefore,

$$\Theta_\Gamma(t) = \begin{cases} \Theta_{start} + \dot{\Theta}_\Gamma t & \text{if} \quad t \leq \tau \\ \Theta_{end} & \text{else} \end{cases}. \tag{7}$$

As for each case, all remaining boundaries are adiabatic, a transformation front will move through the material one-directional. In the tensile testing case, radially from the outer boundary towards the center. For the beam case from bottom to top in height direction. As described above, for the tensile testing case, the upper boundary is fixed vertically. As a result, strains released by the phase transformation will cause stresses, which are quantified by evaluating

$$\overline{\sigma} = \frac{1}{\pi R^2}\left[2\pi \int_0^R \sigma_{zz}(r, z = L_t) r \,\mathrm{d}r\right] = \frac{F}{\pi R^2} \tag{8}$$

via GAUSS-integration. The value of $\overline{\sigma}$ represents the retention force F which is divided by the surface area, meaning it is a surface-averaged stress. Benefit of the chosen boundary conditions is, that in case thermal strains are neglected, it's final value will correspond to $\overline{\sigma} = E\varepsilon_0$.

A classification of the thermal processes is possible by using two dimensionless numbers. The ratio of heat diffusion and heat storage is described by the FOURIER number

$$Fo = \frac{\lambda \tau}{\rho c L^2}. \tag{9}$$

It uses the characteristic length L, which for the tension testing case corresponds to R, for the beam case to H. Note that, in non-isothermal tension experiments, Fo can be influenced by changing the specimen's size and the applied heating rate. For classification of the endothermic phase transformation, latent heat effects need to be captured as well. This is done using the STEFAN number

$$Ste = \frac{c\Delta\Theta_{tr}}{\Delta h_{tr}}. \tag{10}$$

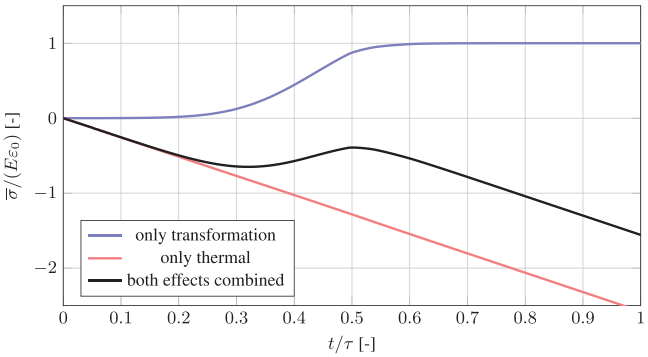

FIGURE 4 Influence of thermal stains in the activation process of a cylindrical sample with $R = 5$ mm at $Fo = 10.26$ and $Ste = 0.21$.

It is the ratio of the caloric heat that is added during phase transformation and latent heat that is consumed by the phase transformation. Note that Ste is a material parameter which means it cannot be influenced by the design of the experiment. Furthermore, to be able to determine it, it is necessary to perform a DSC scan.

The reference parameter setting for the above-mentioned case is $R = 5$ mm and $L_t = 5R$, respectively $H = 0.01$ m and $L_b = 0.1$ m. If thermal strains are considered, the thermal expansion coefficient is set to $\alpha_{th} = 11.8 \times 10^{-6}$ K^{-1}. For achieving a similar magnitude of thermal and transformation strains, $\varepsilon_0 = 1.18 \times 10^{-4}$ was chosen. Such a small value is not the typical use-case for SMAs, however, it allows investigating the interaction between thermal and transformation strains. As a consequence, thermal strains are only considered in the first study presented in the following chapter. For the sake of completeness, it must be noted that in the reference setting, the outer wall's heating rate was set to $\dot{\Theta}_\Gamma = 10$ K s^{-1}. It is quite a large value, however, since it is the aim to perform parameter studies for Fo, the exact value of one parameter is not relevant. It is its relation to other values, as can be seen in Equation (9). The parameters of the phase transformation model were fitted to DSC scans performed for a NiTiHf alloy, which resulted in $\Theta_{tr} = 360.65$ K, $\Delta\Theta_{tr} = 47.75$ K and $\Delta h_{tr} = 114.87$ kJ kg^{-1}, see ref. [4].

4 | STUDY RESULTS

Extensive parameter studies were carried out for the tension testing case. First, the role of thermal strains is investigated. For this reason, the reference case was simulated considering only transformation strains, only thermal strains and both phenomena. The result is plotted in Figure 4. Since transformation strains are causing the sample to contract, tension builds up as the phase transformation front is moving through the sample, as can be seen by the blue curve. Thermal strains are causing the sample to expand, as a result, a compressive state of stress that linearly depends on temperature develops, shown by the red curve. If both phenomena are considered, corresponding to the black curve, it can be seen that they are in superposition and counteract each other. A superposition is expected because of linearity, that thermal strains compensate transformation strains is valuable knowledge if prestrains are small. But as mentioned before, the use case of SMAs are large prestrains, consequently, thermal strains will be magnitudes below. As a result, it can be stated that, a neglection is sufficient in this case. In the following studies, only transformation strains are considered for this reason.

Studies for the FOURIER number are realized by changing the sample's size. Realistic material parameters are used, which means that all simulations were carried out at $Ste = 0.21$. For the given ratio $L_t/R = 5$, R was modified to obtain the Fo-values annotated in Figure 5. As a reference, the 1-D solution is plotted, which corresponds to the solution of Equation (1) for $\Theta = \Theta_\Gamma$ and $\dot{\Theta} = \dot{\Theta}_\Gamma$. Any deviation from this curve is caused by size and latent heat effects. Therefore, it shows the difference to a material point theory, in which it is neglected that the experiment is actually an initial-boundary value problem. The results show that for large FOURIER-numbers, meaning sufficiently small samples or low heating rates, results converge towards the 1-D solution. Note that for the reference case with $R = 5$ mm, $Fo = 10.26$, meaning that samples in this magnitude of dimensions are a suitable choice for the given heating rate. Furthermore, the results show that for too large samples, a pronounced retardation of the stress signal can be expected.

Concluding, the Fo-study shows that if data from tension tests should be used for material modeling or if such experiments should be carried out, it is important to be aware of the Fo-value for the setup. A recommendation would be to use data that was generated at $Fo \gg 10$ respectively designing the setup to ensure this condition. An increase in Fo is more

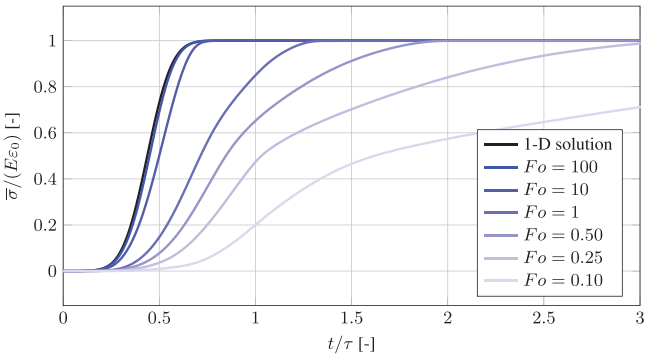

FIGURE 5 Influence of the FOURIER number on the stress signal during activation in the tensile testing case at $Ste = 0.21$. Different values of Fo were realized by varying R.

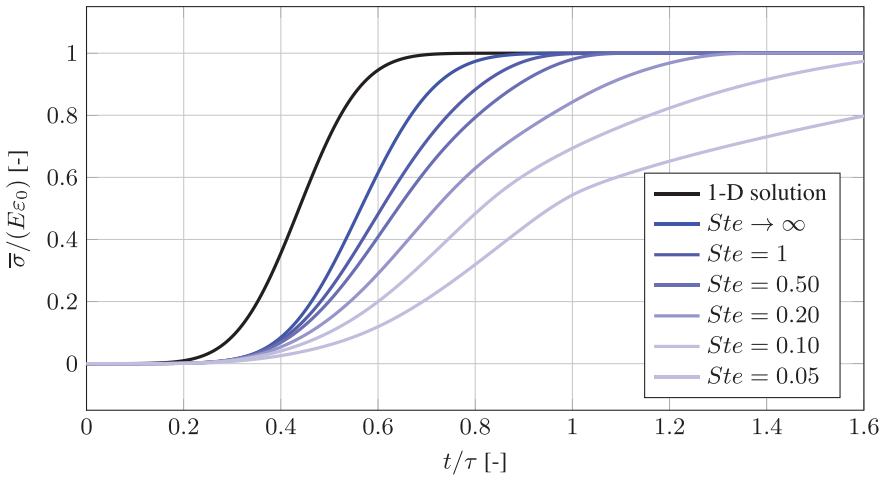

FIGURE 6 Influence of the STEFAN number on the stress signal during activation in the tensile testing case at $Fo = 1$. Different values of Ste were realized by changing Δh_{tr}.

effectively obtained by using smaller samples since R appears quadratically in its denominator. However, a reduction of the heating rate is possible as well.

Investigations about the influence of the STEFAN number are performed by varying Δh_{tr} for a fixed value of $Fo = 1$, which already shows a pronounced deviation from the 1-D solution. Even if latent heat is neglected, as can be seen for the curve for $Ste \to \infty$, a deviation will remain, however, it decreases noticeably. The study shows that if the influence of latent heat is increased, an additional retardation of the stress signal occurs. This means that even if a sufficiently large Fo is ensured by the experimental setup, the material parameter Ste, which cannot be influenced, can falsify experimental data.

In the preceding work [4], the influence of latent heat on the activation process of SMAs is extensively discussed. One major outcome of the studies presented was that, under the influence of latent heat, a transformation front forms. It is pronounced for cases in which large temperature gradients occur, which in the cited work are caused by inductive heating, resulting in a heat shock wave. Only in this case, a sharp interface moves through the geometry, which from a mechanical standpoint means that there is a gradient in transformation strains. Since in the current work, mechanical coupling of the transformation model was realized, for the beam case, the influence of this phenomenon is highlighted. As stated before regarding Figure 3, the phase transformation front moves in height direction of the domain, which is shown in Figure 6. It causes a deflection of the beam towards the heated boundary, which is where the transformation starts. In this region, transformation strains build up first, which leads to a contraction. For the given case, maximum deflection is reached at around $t = 10$ s, which corresponds to the time when the isoline $\phi = 0.5$ passes the center of the domain. After this point, deflection reduces continuously until it completely vanishes at the point the complete domain reaches $\phi = 1$. There is a remaining reduction in the beam's length since the transformation strains are considered volumetric. However, for this example, they are one magnitude smaller than the deflection.

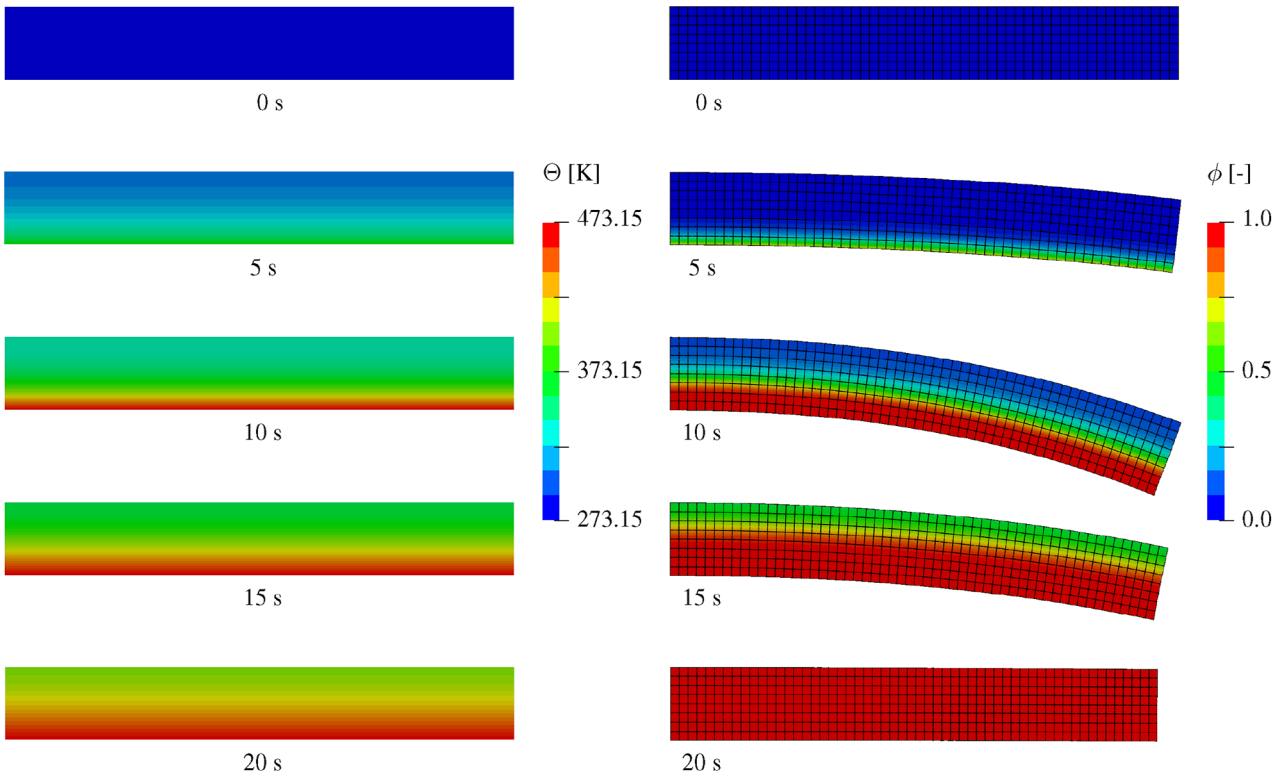

FIGURE 7 Magnified deflection of a beam due to movement of the transformation front in height direction at $Fo = 2.56$ and $Ste = 0.21$.

In the present work, a diffuse interface was observed as well, depicted in Figure 7. As a consequence, in simulations, it should be given attention by solving the energy equation with adequate spatial resolution. Only in this case, the influence of latent heat on the thermal process, which, in turn, influences the position of the interface, is considered correctly. The existence of an interface induces transformation gradients, that have great mechanical influence. One important consequence is that, if desired to derive a beam model, for example, to be able to simulate multi-fiber systems efficiently, it is not possible to neglect these effects. An implementation of the activation direction is obvious for this case since the state of transformation in thickness direction will play a crucial role.

5 | SUMMARY, CONCLUSIONS, AND OUTLOOK

The present work investigates size and latent heat effects in different non-isothermal cases. It focuses on the strain release during the martensite-to-austenite phase transformation in SMAs. The transformation is modelled by a phenomenological evolution equation derived from DSC scans. Its endothermic impact on the energy equation is considered by an enthalpy method, a linear dependency between transformation strains and the martensite-austenite phase indicator is implemented. Studies for a tensile testing case showed that thermal strains counteract transformation strains, but in the use case of SMAs do not play a role. Furthermore, the FOURIER number should be greater than ten, depending on the STEFAN-number even much larger. Results for the activation of a beam in height direction showed that transformation strains will cause bending towards the regions that transform first. The study showed that such effects can only be captured if the energy equation is solved with adequate spatial resolution. A geometrically nonlinear extension of the present work is promising. It would for example, allow studying the process of unfolding for rolled up fibers, described in ref. [10].

ACKNOWLEDGMENTS

Open access funding enabled and organized by Projekt DEAL.

ORCID

Stefan Descher https://orcid.org/0000-0001-9031-7340

REFERENCES

1. Hartl, D. J., & Lagoudas, D. C. (2007). Aerospace applications of SMAs. *Proceedings of the Institution of Mechanical Engineers, Part G: Journal of Aerospace Engineering*, *221*, 535–552.
2. Gerland, F., Schomberg, T., Kuhl, D., & Wünsch, O. (2021). Flow and fiber orientation of fresh fiber reinforced concrete. *Proceedings in Applied Mathematics and Mechanics*, *21*, 202100109.
3. Descher, S., Krooß, P., Ewald, F., Wolf, S., & Kuhl, D. (2023). Latent heat effects in inductive heating of shape memory alloy fibers. *Proceedings in Applied Mathematics and Mechanics*, *23*, e2300300.
4. Descher, S., Krooß, P., Ewald, F., Wolf, S., & Kuhl, D. (2023). Internal prestressing of ultra-high performance concrete using shape memory fibers. *Proceedings in Applied Mathematics and Mechanics*, *23*, e202200253.
5. Marinopoulou, E., & Katakalos, K. (2023). Thermomechanical fatigue testing on Fe-Mn-Si shape memory alloys in prestress conditions. *Materials*, *16*(1), ma16010237.
6. Hong, C., Qian, H., & Song, G. (2020). Uniaxial compressive behavior of concrete columns confined with superelastic shape memory alloy wires. *Materials*, *13*(5), ma13051227.
7. Daghash, S., Ozbulut, O. E., & Sherif, M. M. (2014). Shape memory alloy cables for civil infrastructure systems. *Proceedings of the ASME 2014 Conference on Smart Materials, Adaptive Structures and Intelligent Systems. Volume 1: Development and Characterization of Multifunctional Materials; Modeling, Simulation and Control of Adaptive Systems; Structural Health Monitoring; Keynote Presentation*. Newport, RI, USA, September 8–10, 2014. V001T01A017. ASME., https://doi.org/10.1115/SMASIS2014-7562
8. Voller, V. R., Cross, M., & Markatos, N. C. (1987). An enthalpy method for convection/diffusion phase change. *International Journal for Numerical Methods in Engineering*, *24*, 271–284.
9. Beckermann, C., Diepers, H.-J., Steinbach, I., Karma, A., & Tong, X. (1999). Modeling melt convection in phase-field simulations of solidification. *Journal of Computational Physics*, *154*, 468–496.
10. Schleiting, M., Wetzel, A., Gerland, F., Niendorf, T., Wünsch, O., & Middendorf, B. (2020). Improvement of UHPFRC-rheology by using circular shape memory alloy fibres. In: V. Mechtcherine, K. Khayat, & E. Secrieru (Eds), *Rheology and processing of construction materials*. RheoCon SCC 2019 2019. RILEM Bookseries. Springer. https://doi.org/10.1007/978-3-030-22566-7_17

How to cite this article: Descher, S., Krooß, P., Ewald, F., & Kuhl, D. (2024). Thermomechanical analysis of strain recovery in shape memory alloys under variable non-isothermal conditions. *Proceedings in Applied Mathematics and Mechanics*, *24*, e202400203. https://doi.org/10.1002/pamm.202400203